

Pyramidal Si nanocrystals with a quasiequilibrium shape selectively grown on Si(001) windows in ultrathin SiO₂ films

Motoshi Shibata,* Yoshiki Nitta, Ken Fujita,† and Masakazu Ichikawa

Joint Research Center for Atom Technology, Angstrom Technology Partnership (JRCAT-ATP), 1-1-4 Higashi, Tsukuba, Ibaraki 305-0046, Japan

(Received 18 October 1999)

Pyramidal Si nanocrystals selectively grown on Si(001) windows in ultrathin 0.3-nm-thick SiO₂ films were studied using *in situ* scanning tunneling microscopy. In the initial growth stage, {1, 1, 13} facets were formed on the four equivalent sidewalls of the crystal due to the repulsion force between neighboring steps. The crystals were stable with a quasiequilibrium shape when they were surrounded by the SiO₂ film, but rapidly decayed once the boundary to the SiO₂ film was removed. This indicates that Si adatoms were confined within the Si window area by the surrounding ultrathin SiO₂ film and the Si adatom density became stationary. The confinement was enabled by a difference in the adsorption energy of Si adatoms on SiO₂ and these on Si(001).

I. INTRODUCTION

Selective growth on a patterned silicon dioxide (SiO₂) surface is an important technique for fabricating well-ordered nanostructures in given areas. Si selective growth has generally been done using gaseous sources¹⁻³ because gaseous sources dissociate only on window areas where Si surfaces are exposed. On Si(001) surfaces, Si epitaxial crystals showed a pyramidal shape with four equivalent facets: {1,1,1},^{1,2} {1,1,3},¹⁻³ and {1,1,9} planes.² Facet formation is a promising approach for simultaneously fabricating fluctuationless and similar structures. We recently grew a different type of pyramidal crystals, whose sidewalls have a more gradual slope, on nanometer-scale Si(001) surface windows in ultrathin 0.3-nm-thick SiO₂ films (the top Si layer was oxidized).^{4,5} (001) terraces were clearly observed on the sidewalls of these crystals. In a previous study by Hirayama *et al.*,³ they proposed a {1,1,1} and {1,1,3} facet formation mechanism, and indicated that reducing the number of dangling bonds and the strain is important to form these facets, where growth in the lateral directions is restricted by SiO₂ films. On the other hand, the gradual facets of pyramidal crystals are regarded as an assembly of well-ordered (001) terraces since the terrace widths are large compared with those of {1,1,1} and {1,1,3} surfaces. Hence, we consider the step-step interaction between the neighboring steps to be essential to form the facets.

From the shape of micrometer-scale Si droplets, Bermond *et al.*⁶ determined the equilibrium shape of a Si crystal, and obtained a Si surface-energy curve as a function of crystal misorientation. The equilibrium condition was established only around the Si droplets. In their study, the surface energy increased from (001) to {1,1,1} via the {1,1,3} plane, and had local minimums at the {1,1,1} and {1,1,3} planes. A selectively grown crystal with {1,1,3} facets also seemed to have an equilibrium shape. However, on large clean Si surfaces during annealing, artificial Si nanostructures⁷⁻¹⁰ have always decayed independently of the nanostructure shapes with different facets. These decay processes were caused by the dif-

ference in Si adatom concentration between the steps on the flat surface and the nanostructures. When selectively grown crystals surrounded by SiO₂ films are stable during annealing, the crystals are thought to be under a quasiequilibrium condition. To maintain the quasiequilibrium condition, the concentration of Si adatoms must be preserved and becomes stationary within window areas. In our recent studies, we have found that selectively grown crystals having gradual facets are stable during annealing. Hence, the SiO₂ film has to prevent a decrease in the Si adatoms concentration within a window area. That is why the role of the SiO₂ film in selective growth and annealing of the Si crystals is important to understand. The stability of the crystals is essential when forming heteronanostructures since various materials, such as layers of Ge or other metals, will be overgrown at elevated temperatures.

In this paper, we report on our *in situ* scanning tunneling microscopy (STM) study of the mechanism of facet formation in the very early stage, the quasiequilibrium shape of the Si crystals at elevated temperatures, and the effect of the SiO₂ film on the Si crystals.

II. EXPERIMENT

Well-oriented *n*-type Si(001) wafers were used in this study. Details of the experimental sequences and the apparatus are described elsewhere.^{4,5,11} After the sample was flash heated several times at 1200 °C, a 0.3-nm-thick SiO₂ film was formed in an atmosphere of molecular oxygen at a pressure of 2×10^{-6} Torr at 630 °C for 10 min. Si windows in the SiO₂ film were fabricated by two methods. The first method used thermal decomposition of the SiO₂ film.⁴ During annealing at 700–730 °C, the SiO₂ film started to decompose, and rectangular Si(001) windows (elongated in the $[\bar{1}10]$ and $[110]$ directions) appeared and then expanded in the voids of the SiO₂ film. When the sizes of the voids were 10–40 nm, the annealing was stopped and the sample temperature was decreased to the growth temperature. The windows were randomly distributed over the surface. The sec-

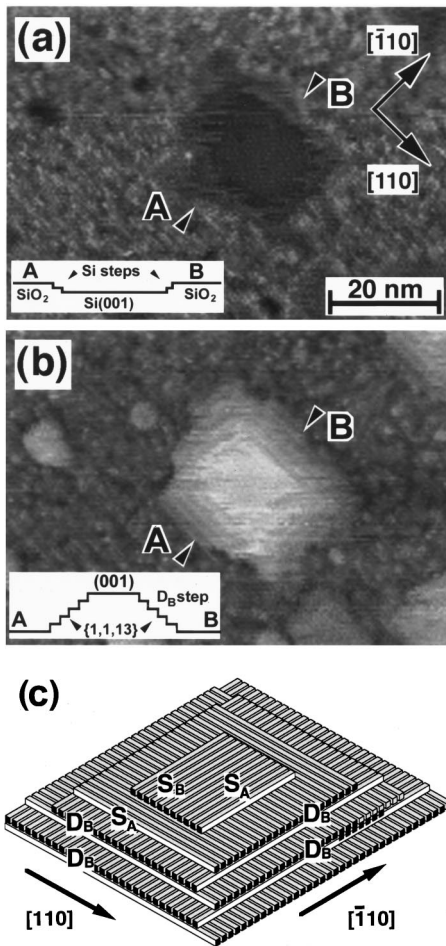


FIG. 1. Typical STM images of selective growth on a Si(001) window at 600 °C: (a) before growth, and (b) 12 min after Si growth started. The insets show schematic height differences along lines A–B. The configuration of the S_A , S_B , and D_B steps on a pyramidal crystal is schematically shown in (c). Cuboids represent the dimer rows.

ond method used electron-beam-induced thermal decomposition.^{5,12} During annealing at 550–630 °C, the oxidized Si surfaces were irradiated with field-emission (FE) electron beams from an STM tip with an energy of 70–150 eV and a current of 10–50 nA. In the irradiated area, the composition of SiO₂ was changed to SiO due to electron-stimulated desorption (oxygen desorbed from the SiO₂ films). The SiO in the film was easily volatilized, and then the window areas in the SiO₂ film were exposed. This method can be used to fabricate the SiO₂ film in a given area, and allows atomic-scale imaging immediately after the fabrication. After the window fabrication, selective growth was performed using disilane (Si₂H₆) at 550–630 °C. The Si₂H₆ dose rate was from 3.3×10^{-7} to 2.6×10^{-6} Torr. In order to obtain stable oxide surface images,⁴ all the STM images were taken at a tunneling current of 60 pA and a sample bias voltage of +4.0 V.

III. RESULTS AND DISCUSSION

A. Pyramidal crystals

Figure 1 shows typical STM images of the Si selective growth at 600 °C. The height differences are schematically

shown as insets. The Si₂H₆ dose rate was 3.3×10^{-7} Torr. Figure 1(a) shows an oxidized Si(001) surface after windows were fabricated by thermal decomposition of the SiO₂ film. The dark and bright contrast areas correspond to Si(001) windows and the SiO₂ film, and almost all the windows are rectangular with their sides parallel to the $[\bar{1}10]$ and $[110]$ directions.⁴ The windows are hollow because the decomposition of the SiO₂ film requires additional Si atoms from the substrate [$\text{SiO}_2 + \text{Si} \rightarrow 2\text{SiO}$ (volatile)]. Since Si monoatomic steps move more quickly than the STM tip scan frequency, the steps in the windows area look like zigzag lines. The step structures on Si(001) surfaces are classified into four types (S_A , S_B , D_A , and D_B): $S(D)$ indicates the single- (double-) step height and $A(B)$ indicates the step direction parallel (perpendicular) to the dimer row direction on the upper terrace.¹³

Figure 1(b) shows an STM image taken after 12 min of growth at 600 °C. Si crystals are epitaxially grown on all the windows. While the small crystals (less than 10 nm in size) are irregular, the larger crystals have a pyramidal shape. The height of the crystal in the center of the image is 12 monolayers (ML) from the bottom of Fig. 1(a). On the four equivalent sidewalls, there are D_B steps with intervals of about $6.5a_0$, where a_0 is the lattice constant of the (001) surface (0.38 nm). The slope angle and the terrace width of the $\{11n\}$ facet are expressed, respectively, by $\tan^{-1}[\sqrt{2}/n]$ and $(na_0/2)$. The sidewalls therefore consist of a $\{1,1,13\}$ plane. Our STM images of the $\{1,1,13\}$ facets at room temperature agree well with those of vicinal Si(001) surfaces obtained by Baski *et al.*¹⁴ The configuration of the S_A , S_B , and D_B steps on a pyramidal crystal is schematically shown in Fig. 1(c). Cuboids represent the dimer rows. Ridges of the pyramidal crystal between neighboring $\{1,1,13\}$ planes are unclear in the high-temperature STM image. Because D_B steps on different sidewalls (along the $[\bar{1}10]$ and $[110]$ directions) are not at the same height, stable structures are probably not formed along the ridges. In the Si₂H₆ dose rate range from 3.3×10^{-7} to 2.6×10^{-6} Torr, further growth transformed $\{1,1,13\}$ into $\{11n\}$ ($n = 11, 9, 7, 5, 3$) facets while the $\{1,1,1\}$ facet could not be seen. In a previous study of $\{1,1,13\}$ facet formation at 550 °C by Hirayama *et al.*,³ the maximum dose rate was about 65% higher than our maximum dose rate, and their and our experimental conditions are within the Si₂H₆ flow-rate-limiting regime. Hence, the formation of the $\{1,1,n\}$ facets depends on the growth time, not the growth rate. In our experiment, $\{1,1,1\}$ facet formation requires a much longer growth time, since the $\{1,1,1\}$ facets were only observed after overgrowth of the surrounding SiO₂ films;^{1,2} the grown crystals touched the SiO₂ films. During epitaxial growth using Si₂H₆, surface dangling bonds are terminated by hydrogen, and the growth rate is dominated by the thermal desorption rate of hydrogen near the hydrogen-desorption temperature. Temperature-programmed-desorption mass spectrometry revealed that the hydrogen-desorption yield peaked at 540 °C.¹⁵ Therefore, hydrogen does not affect the surface structures under our experimental conditions. Hence, $\{1,1,13\}$ facet formation is an essential process in the early stage of Si selective growth.

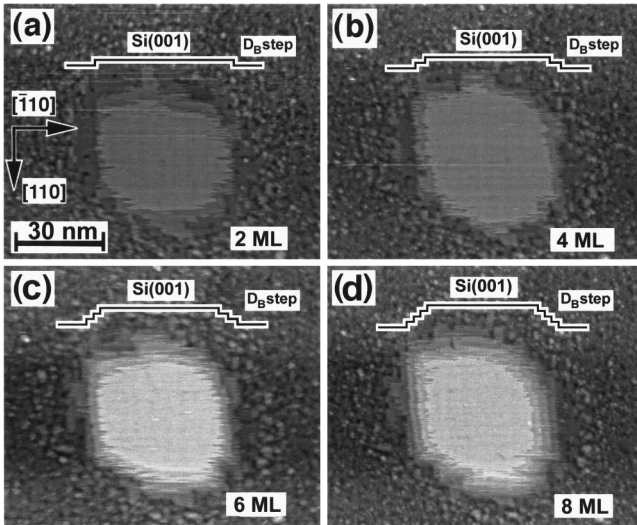


FIG. 2. Sequential STM images of selective growth at 600 °C. The crystal height is (a) 2 ML, (b) 4 ML, (c) 6 ML, and (d) 8 ML.

Figure 2 shows sequential STM images of Si selective growth at 600 °C. The round window (about 35 nm in diameter) was fabricated with an FE electron beam from the STM tip. The height differences in the $[\bar{1}10]$ direction are schematically shown as insets. The Si_2H_6 dose rate was 3.3×10^{-7} Torr. Figure 2(a) shows a two-dimensional (2D) island 2 ML in height grown on the center of the window. D_B steps along the $[110]$ direction are already formed on the left and right sides of the window. Since S_B steps grow much faster than S_A steps, the S_B (higher) step overtakes, and combines with the S_A step (lower), thus forming D_B steps.¹⁶ The D_B step is an energetically favorable structure where the miscut angle is more than 2° – 3° (the terrace width is 7.5–5.2 nm).¹⁷ At the top and bottom sides of the window, two pairs of S_B and S_A steps run along the $[\bar{1}10]$ direction. The lower and higher steps, respectively, are S_B and S_A steps. Since the D_A step is an energetically unfavorable structure,¹³ D_A step edges are not formed along the $[\bar{1}10]$ directions; the S_B (lower) and S_A (higher) steps are not combined. Figures 2(b), 2(c), and 2(d) show 2D islands, which are, respectively, 4, 6, and 8 ML in height, which grow in the window area. On the left and right sides of the 2D islands, all the D_B steps are bunched. In Fig. 2(d), the $\{1,1,13\}$ facet is completely formed. Although D_B steps along the $[\bar{1}10]$ direction are unclear in this image, since the STM tip scan direction is parallel to the step direction, the $\{1,1,13\}$ facets are also formed on the sidewall as shown in Fig. 1(b). As shown in Fig. 1(c), the accumulation order of the monoatomic steps along the $[\bar{1}10]$ directions is $S_B, S_A, S_B, S_A, \dots$ (from bottom to top). The S_A and S_B steps, except for the lowest S_B step, combine with each other, forming the D_B steps along the $[\bar{1}10]$ directions.

B. Formation mechanism of pyramidal crystals

Although the crystals in our experiment had a pyramidal shape, we use the simplest possible model in order to explain the growth mechanism of the crystal. In this model, the crystal consists of a stack of round 2D islands with radius R_i ,

and the step-step repulsion force is ignored. Each island step edge has a Gibbs-Thomson chemical potential μ_i^s ($=a_0^2\tilde{\beta}/R_i$), where $\tilde{\beta}$ is the step-edge stiffness. The growth rate of the i th islands area is given by $dA_i/dt = -2\pi R_i\Gamma\Delta\mu_i/(a_0^2kT)$, where Γ is the step mobility.¹⁸ $\Delta\mu_i$ is the difference of the chemical potential ($\mu_i^s - \mu_i^{ad}$), where μ_i^{ad} is the chemical potential of Si adatoms on the i th terrace. During growth, since the Si adatom concentration increases, μ_i^{ad} becomes larger than μ_i^s , so the signs of $\Delta\mu_i$ and dA_i/dt , respectively, become negative and positive. Where the crystal is surrounded by a SiO_2 film, growth of a base island is restricted by the SiO_2 film. Hence, during selective growth, each R_i becomes larger and the sidewall slope steepens; thus the terrace widths become smaller. The driving force of the faceting is the increased chemical potential of the Si adatom.

Based on the shape of nanometer-scale voids in Si bulk crystal and micrometer-scale Si droplets, Eaglesham *et al.*¹⁹ and Bermond *et al.*⁶ have reported that the Si surface energy is a function of crystal misorientation; the surface energy increases from (001) to $\{1,1,1\}$ via the $\{1,1,3\}$ plane. The surface energy of Bermond *et al.* had local minimums at the $\{1,1,1\}$ and $\{1,1,3\}$ planes. When the miscut angle from (001) is small, Poon *et al.*²⁰ has attributed the increased surface energy to step-step repulsion between neighboring D_B steps. Using the Stillinger-Weber empirical potential, they calculated the surface energy on vicinal Si(001) surfaces as a function of terrace width l : $\lambda(l) = \lambda_{D_B} + \lambda_d(a_0/l)^2$, where λ_{D_B} and λ_d are, respectively, the step-formation energy ($-42 \text{ meV}/a_0$) and the step-step repulsion ($1271 \text{ meV}/a_0$). Since this surface energy is defined as the difference from the energy of the cascade of a single-stepped surface without domain-stress and step-step interactions, the step-formation energy cannot be directly compared with the experimental values obtained by Eaglesham *et al.*¹⁹ ($46 \text{ meV}/a_0$) and Zandvliet *et al.*²¹ ($50 \text{ meV}/a_0$) because the reference systems are different from each other. However, the theoretical result obtained by Poon *et al.* explains well the critical miscut angle ($\sim 1.5^\circ$) between single- and double-stepped (D_B) surfaces; the latter is energetically favorable when the miscut angle is larger than the critical value. Hence, the theoretical result is applied to evaluate the surface energy on vicinal surfaces. The surface energy $\lambda(l)$ rises rapidly as the miscut angle increases up to 5° (corresponding to the $\{1,1,15\}$ facet). This indicates that the decrease in the terrace widths is limited by the increasing surface energy due to the step-step repulsion, even though the decreasing width is caused by the increasing chemical potential of the Si adatom. On the $\{1,1,(2n+1)\}$ ($n \geq 3$) plane, well-ordered D_B steps have been clearly observed,¹⁴ and we did not observe the $\{1,1,2n\}$ facets during growth. These observations suggest that an activation-energy barrier E_{step} exists between the $\{1,1,(2n-1)\}$ and $\{1,1,(2n+1)\}$ facets. Thus, local minimums of the surface energy probably exist on the $\{1,1,(2n+1)\}$ plane, although they were not clearly observed by Bermond *et al.*⁶ Referring to the difference in the step energy [$=\lambda(l_{11}) - \lambda(l_{13})$], the activation energy barrier per lattice constant is at least $12 \text{ meV}/a_0$; this value must be the minimum. Hence, we consider that $\{1,1,13\}$ facets are

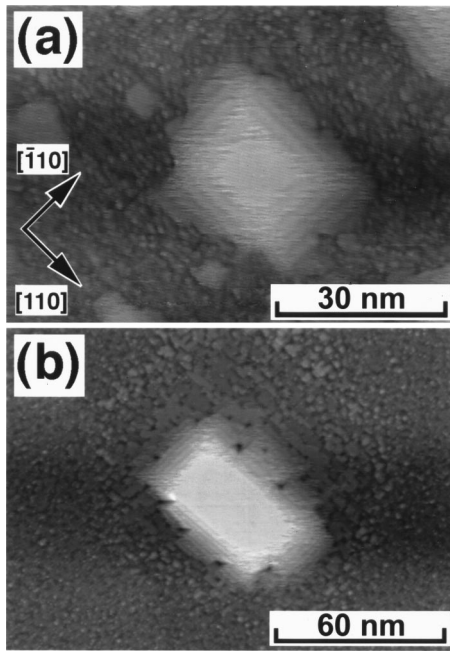


FIG. 3. Typical STM images of a pyramidal crystal during annealing at 600 °C: (a) 34 min and (b) 10 min after Si growth stopped. Window areas in (a) and (b) are fabricated by thermal decomposition and an FE electron beam from the STM tip, respectively.

formed on the sidewalls when the adatom chemical potential is insufficient to overcome the activation-energy barrier.

C. Stability of pyramidal crystals

Figure 3(a) shows an STM image of the sample shown in Fig. 1(b) after 34 min annealing at 600 °C. During annealing, the pyramidal Si crystal shape is preserved. It seems that the pyramidal crystals have a quasiequilibrium shape, and that the SiO₂ film can restrict the outflow of Si adatoms from the window area. However, we have to pay careful attention to two kinds of Si adatom attachment and detachment processes. One process is related to the interchange of adatoms between the neighboring crystals since the distances between the neighboring crystals are small (10–30 nm). The other process is related to the effect of the STM tip since the tip is only about 1 nm apart from the surface and is usually covered with surface material (Si). To investigate the former process, we fabricated an isolated window by using an FE electron beam from the STM tip, and observed the effect of annealing on the shape of the crystal. Where the interchange of Si adatoms is allowed, the adatoms that detach from the crystal will spread over the surface. The crystal must then decay during annealing. Figure 3(b) shows an STM image of a pyramidal crystal after 10 min annealing at 600 °C. In this image, the sidewalls consist of {1,1,13} facets. Therefore, the interchange of Si adatoms is prohibited, and the crystal shape is unaffected by the neighboring crystals. Concerning the latter process, Ichimiya *et al.*⁸ reported that the decay rates of artificial Si structures on a flat clean Si surface are affected by STM observation. They found that the interchange between Si adatoms on the STM tip and those on the Si structures increases the decay rates, but hardly affects the equilibrium condition. Moreover, with and without *in situ*

STM observation, we observed pyramidal crystals with {1,1,13} facets after 2 h of annealing at 600 °C. We therefore conclude that the Si crystals have a quasiequilibrium shape, and that Si adatoms are confined within the Si window area. Since the SiO₂ film is 0.3 nm thick, the confinement was caused not by the geometrical barrier, but by the potential barrier between SiO₂ and Si(001) surfaces. We consider that the energy barrier originates from the difference in the adsorption energy of adatoms on SiO₂ and those on Si surfaces. Such a potential barrier has been reported in a study of aluminum adatom preferential migration toward bare Si areas on H-terminated Si(111) surfaces.²²

In Figs. 1(b) and 3(a), the difference in volume of the pyramidal crystals is quite small ($\leq 1-10\%$) after 34 min(*t*) annealing at 600 °C. The number of Si adatoms overcoming the potential energy barrier (E_{SiO_2}) along the boundary between the Si crystal and the SiO₂ film is given by $n = n_0 t \nu \exp[-E_{\text{SiO}_2}/kT]$ when hopping frequency $\nu \sim 10^{13}/\text{s}$ (n_0 initial number of Si adatoms). When $n \leq n_0/100(n_0/10)$, E_{SiO_2} is estimated to be at least 3.24 (3.07) eV. Using a first-principles calculation, Yamasaki and Uda²³ obtained 5.12 eV for the adsorption energy of Si adatoms on Si(001) surfaces. Although the adsorption energy on SiO₂ film is not known for certain, it is thought to be very small because a SiO₂ film surface is chemically inert. Hence, for Si adatoms, the energy barrier is $3.24 (3.07) \text{ eV} < E_{\text{SiO}_2} < 5.12 \text{ eV}$. This energy barrier reflects the adatoms detached from the step edge of the crystals, and confines the adatoms within the window area.

Tanaka *et al.*,¹⁰ Bartelt *et al.*,¹⁸ and Natori *et al.*²⁴ found that hillocks and holes decay on a clean Si surface during annealing. These decay processes are caused by a difference in Si adatom concentration at the step edges on the flat surface and those on the hillocks and holes. In order to understand the decay mechanism of the crystal, we again use the simplest model: a stack of round 2D islands. When the crystal decays spontaneously, the chemical potential of Si adatoms on the *i*th terrace μ_i^{ad} is small compared with the Gibbs-Thomson chemical potential μ_i^{s} , so $\Delta\mu_i$ has a positive sign. With a decreasing radius R_i , the difference in the chemical potential $\Delta\mu_i$ increases. This difference in $\Delta\mu_i$ causes a difference between the Si adatom concentrations at the top and bottom of the crystal, so the direction of the adatom diffusion is from top to bottom. The island at the top of the pyramidal crystal decays easily. The decay rate of the top island area is given by $dA_1/dt = -2\pi R_1 \Gamma \Delta\mu_1 / (a_0^2 kT)$. When the island area is small enough, $\mu_1^{\text{s}} \gg \mu_1^{\text{ad}}$, the decay rate is estimated to be about 630 nm²/s, where $T = 600 \text{ °C}$, $\tilde{\beta} \sim 0.15 \text{ eV/nm}$,²⁵ and $\Gamma \sim 50 \text{ nm}^3/\text{s}$.¹⁸ The $\tilde{\beta}$ and Γ for the S_A step are used since the top island steps partly consist of the S_A step, as shown in Fig. 1(c). The decay rate is similar to that of Si islands on Si(001), estimated from lower-temperature results reported by Ichimiya *et al.*⁸ The step-step repulsion force produces an additional chemical potential μ_i^{r} at the step edges, which increases the decay rate of the crystal.^{10,26} Si crystals thus decay rapidly on a clean surface, while pyramidal crystals surrounded by SiO₂ film in our experiment do not. This indicates that the adatom chemical potential μ_i^{ad} is nearly

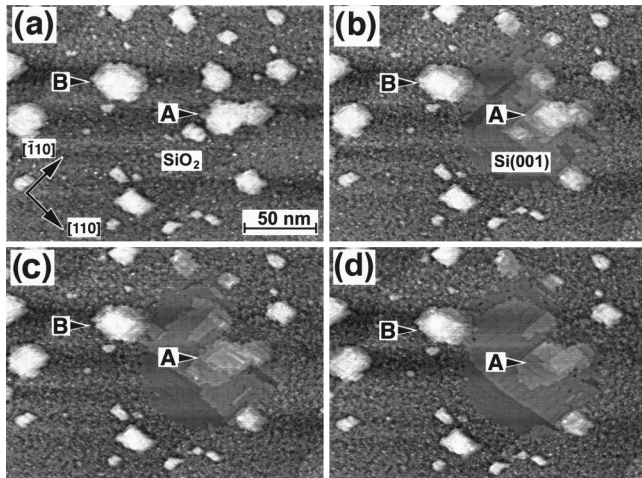


FIG. 4. STM images before and after selective removal of the SiO_2 film surrounding the pyramidal crystals at 430°C : (a) before fabrication, (b) 2.5 min, (c) 8.5 min, and (d) 38 min after fabrication.

equal to the sum of the Gibbs-Thomson chemical potential μ_i^s and the step-step repulsion chemical potential μ_i^r . Since Si adatoms are confined within the Si window area by the potential barrier, the adatoms are reflected at the barrier, and the Si adatom density became stationary within the Si window area.

D. Decay of pyramidal crystals

Figure 4(a) shows an STM image taken at 430°C after selective growth at 550°C . Figures 4(b), 4(c), and 4(d) are images taken 2.5, 8.5, and 38 min after selective removal of the SiO_2 film with an FE electron beam from the STM tip at 430°C . The electron-beam irradiation might have affected the Si crystals, as well as the SiO_2 film. For example, the substrate temperature could have risen due to the electron-beam irradiation. Therefore, we focus on the difference between Figs. 4(b), 4(c), and 4(d). The SiO_2 -film-removed area is about 100 nm in diameter. The surface is divided into three regions according to the border between the SiO_2 film and the area where the SiO_2 film was removed [the Si(001) surface]: inside, along, and outside the border. The Si pyramidal crystals indicated by arrows A and B are inside and along the border. Inside the border in Fig. 4(b), a Si(001) surface with small holes and hillocks can be seen. These small holes are formed when the electron dose is insufficient,⁵ and the hillocks correspond to the pyramidal crystal shown in Fig. 4(a). In Figs. 4(c) and 4(d), the hillocks can still be seen, but their heights become lower. Moreover, the small holes disappear and the step edges of large 2D islands become smoother. These features indicate that Si-adatom migration occurs due to the difference between the Si-adatom concentration at the step edges on the flat surface and that at the hillock and hole edges. In Figs. 4(b)–4(d), the crystal denoted by A decays from the top of the crystal while the area of the base is almost unchanged. This decay process agrees well with a previous study by Tanaka *et al.*¹⁰ which showed that Si layers disappear from the top of the crystal. Enlarged images and height profiles in the [010] direction of crystal B are shown in Figs. 5 and 6, respectively. In Fig.

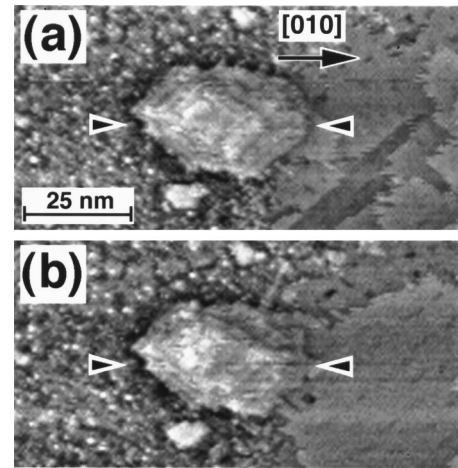


FIG. 5. Enlarged STM images of crystal A in Fig. 4: (a) 2.5 min and (b) 38 min after fabrication.

6(b), the thin line indicates the height profile 2.5 min after the selective removal of the SiO_2 film. In Fig. 5(a), the right side of the crystal faces the Si exposed area while the left side does not. In Fig. 5(b), the right half of the crystal decayed while the left half did not. The height profiles of the crystals in Fig. 6 also indicate that only the right half of the crystal decayed. Moreover, the crystal decays from the top and the base of the crystal is almost unchanged. This decay process is described by the simple-island model; the island at the top of the crystal decays easily due to the difference in the Gibbs-Thomson chemical potential μ_i^s depending on the radius R_i . On the right side of the crystal, the Si adatoms of the crystal diffuse from the top of the crystal due to the difference between the Si-adatom concentration at the step edges on the flat surface and that of the crystal. However, on the left side of the crystal, Si adatoms are reflected at the boundary between the Si crystal and the SiO_2 film, and do not spread over the surface. These results indicate that the crystals were stable when they were surrounded by a SiO_2 film, but rapidly decayed in the same manner on clean surfaces once the boundary to the SiO_2 film was removed. We therefore consider that the pyramidal crystals are preserved in a quasiequilibrium shape during annealing.

IV. SUMMARY

We studied the selective growth and annealing of a pyramidal crystal on Si surface windows in an ultrathin SiO_2

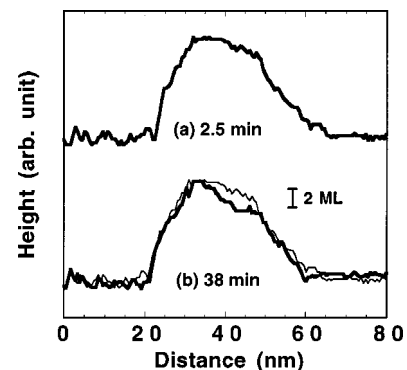


FIG. 6. Height profiles along the [010] direction in Fig. 5, as indicated by arrows: (a) 2.5 min and (b) 38 min after fabrication. The thin line in (b) indicates the height profile at 2.5 min.

film. The crystal had a quasiequilibrium shape, and its sidewall consisted of $\{1,1,13\}$ facets. The facet formation appears to depend on the step-step repulsion force. Moreover, the crystal was stable when they were surrounded by a SiO_2 film, but rapidly decayed once the boundary between the Si crystal and the SiO_2 film was removed. This indicates that the ultrathin SiO_2 film prevented Si adatoms from spreading over the surface and kept the concentration of the adatoms within the window area stationary. Such stable Si nanocrystals will be necessary to form Si-based nanostructures at elevated temperatures.

ACKNOWLEDGMENTS

The authors wish to thank Dr. N. Miyata, Dr. T. Yamasaki (Fujitsu Laboratory), Dr. T. Uchiyama, and T. Uda for helpful discussions. This work, partly supported by New Energy and Industrial Technology Development Organization (NEDO), was performed by the Joint Research Center for Atom Technology (JRCAT) under an agreement between the National Institute for Advanced Interdisciplinary Research (NAIR) and the Angstrom Technology Partnership (ATP).

*Electronic address: shibata@jrcat.or.jp

[†]Present address: Oki Electronic Industry Co., Ltd., Hachioji, Tokyo 193-8550, Japan.

¹T. Aoyama, T. Ikarashi, K. Miyanaga, and T. Tatsumi, *J. Cryst. Growth* **136**, 349 (1994).

²L. Vescan, K. Grimm, and C. Dieker, *J. Vac. Sci. Technol. B* **16**, 1549 (1998).

³H. Hirayama, M. Hiroi, and T. Ide, *Phys. Rev. B* **48**, 17 331 (1993).

⁴K. Fujita, H. Watanabe, and M. Ichikawa, *Appl. Phys. Lett.* **70**, 2807 (1997).

⁵M. Shibata, Y. Nitta, K. Fujita, and M. Ichikawa, *Appl. Phys. Lett.* **73**, 2179 (1998).

⁶J.M. Bermond, J.J. Métois, X. Egéa, and F. Floret, *Surf. Sci.* **330**, 48 (1993).

⁷M. Iwatsuki, S. Kitamura, T. Sato, and T. Sueyoshi, *Appl. Surf. Sci.* **60/61**, 580 (1992).

⁸A. Ichimiya, Y. Tanaka, and K. Hayashi, *Surf. Sci.* **392**, 182 (1997).

⁹T. Ogino, H. Hibino, and Y. Homma, *Jpn. J. Appl. Phys., Part 2* **34**, L668 (1995).

¹⁰S. Tanaka, N.C. Bartelt, C.C. Umbach, R.M. Tromp, and J.M. Blakely, *Phys. Rev. Lett.* **76**, 4721 (1996).

¹¹K. Fujita, Y. Kusumi, and M. Ichikawa, *Surf. Sci.* **380**, 66 (1997).

¹²N. Li, T. Yoshinobu, and H. Iwasaki, *Jpn. J. Appl. Phys., Part 2* **37**, L995 (1998).

¹³D.J. Chadi, *Phys. Rev. Lett.* **59**, 1691 (1987).

¹⁴A.A. Baski, S.C. Erwin, and L.J. Whitman, *Surf. Sci.* **392**, 392 (1997).

¹⁵S.M. Gates, R.R. Kunz, and C.G. Greenlife, *Surf. Sci.* **207**, 364 (1989).

¹⁶A.J. Hoeven, J.M. Lenssinck, D. Dijkkamp, E.J. van Loenen, and J. Dieleman, *Phys. Rev. Lett.* **63**, 1830 (1989).

¹⁷P.E. Wirenga, J.A. Kubby, and J.E. Griffith, *Phys. Rev. Lett.* **59**, 2169 (1987).

¹⁸N.C. Bartelt, W. Theis, and R.M. Tromp, *Phys. Rev. B* **54**, 11 741 (1996).

¹⁹D.J. Eaglesham, A.E. White, L.C. Feldman, N. Moriya, and D.C. Jacobson, *Phys. Rev. Lett.* **70**, 1643 (1993).

²⁰T.W. Poon, S. Yip, P.S. Ho, and F.F. Abraham, *Phys. Rev. B* **45**, 3521 (1992).

²¹H.J.W. Zandvliet, S. van Dijken, and B. Poelsema, *Phys. Rev. B* **53**, 15 429 (1996).

²²N. Enomoto, T. Hoshino, M. Hata, and M. Tsuda, *Appl. Surf. Sci.* **130-132**, 132 (1998).

²³T. Yamasaki and T. Uda (private communication); in their work [*Phys. Rev. Lett.* **76**, 2949 (1996)], they calculated the adsorption energy of one Si adatom on a $\text{Si}(001) c(4 \times 2)$ surface (5.12 eV/atom).

²⁴A. Natori, M. Murayama, D. Matsumoto, and H. Yasunaga, *Surf. Sci.* **409**, 160 (1998).

²⁵N.C. Bartelt and R.M. Tromp, *Phys. Rev. B* **54**, 11 731 (1996).

²⁶E.S. Fu, D.-J. Liu, M.D. Johnson, J.D. Weeks, and E.D. Williams, *Surf. Sci.* **385**, 259 (1997).